Ab initio and semiempirical dielectric response of superlattices

Silvana Botti,* Nathalie Vast, Lucia Reining, and Valerio Olevano
Laboratoire des Solides Irradiés, CNRS-CEA-École Polytechnique, F-91128 Palaiseau, France

Lucio Claudio Andreani
INFM–Dipartimento di Fisica "A. Volta," Università di Pavia, Via Bassi 6, I-27100 Pavia, Italy
(Received 22 December 2003; published 2 July 2004)

We present a study of the dielectric response of $(GaAs)_p/(AlAs)_p$ (001) superlattices in a wide range of barrier and well widths. We applied density functional theory and a semiempirical method to obtain the superlattice band structures. These were then used as a starting point to evaluate the optical spectra and macroscopic dielectric constants using time-dependent density functional theory. In this context, we investigated the role of crystal local field effects in determining the anisotropy of the dielectric constants. Furthermore, we calculated absorption spectra including the strong continuum excitonic effect through the use of an appropriate model exchange-correlation kernel. We analyzed in detail the complementarity of the *ab initio* and semiempirical approaches and we compared the successes and limitations of the different approximation schemes.

DOI: 10.1103/PhysRevB.70.045301 PACS number(s): 73.21.Cd, 78.20.Fm, 78.20.Bh, 78.66.Fd

I. INTRODUCTION

Reducing the size of one-, two-, or three-dimensional heterostructures at the nanoscale level leads to electronic ground and excited states widely different from those of the bulk crystals, and has opened the way to a new generation of optoelectronic and photonic devices. In nanostructured materials, the electronic states vary from those of the bulk constituents essentially due to three effects. (i) The band offsets at the interfaces act as effective potential barriers, inducing the confinement of carriers (both electrons and holes) in potential wells. (ii) As a consequence of the creation of a supercell in the direct space, in reciprocal space the bulk bands are folded onto a smaller Brillouin zone. This back folding is accompanied by the mixing of otherwise independent bulk states, coupled by the superimposed confining potential. (iii) The composite crystal can exhibit symmetry breaking with respect to its building blocks: in particular, the lowering of an original cubic symmetry gives rise to anisotropy in the electronic properties.

GaAs/AlAs superlattices (SL's) are prototypes of semiconducting heterostructures and have been extensively studied, both experimentally[1–3] and theoretically,[4–10] in recent years. The original point group of GaAs and AlAs bulk crystals is the T_d group of zinc blende, which yields an isotropic optical response of the medium. When a multilayer with a common-ion interface is grown along the [001] crystalline axis, the original cubic T_d symmetry is reduced to tetragonal D_{2d}. The system turns from isotropic into uniaxial, with a macroscopic dielectric tensor containing two components $\varepsilon_\parallel$ and $\varepsilon_\perp$, describing the response for light polarized along the growth direction and in the plane containing the interfaces. The anisotropy of GaAs/AlAs-based SL's, together with the huge second-order susceptibility of GaAs, have been successfully applied in the design of frequency converters.[11] These devices, working at frequencies in the infrared region, exploit the change in the refractive index with light polarization—the birefringence $\Delta n(\omega)=\sqrt{\varepsilon_\perp(\omega)}-\sqrt{\varepsilon_\parallel(\omega)}$—to prevent optical dispersion. This is achieved by matching the phase velocities for light propagating at different frequencies. Below the energy gap, while approaching the first allowed dipole transition, the birefringence is dominated by resonant contributions. On the other hand, in the low-frequency region $\Delta n(\omega)$ is rather dispersionless and can be well approximated by its zero-frequency value $\Delta n(0)$. The magnitude of the static birefringence $\Delta n(0)$ is related to the dielectric mismatch of the constituent crystals, and shows a nontrivial dependence on the barrier and well width. In particular, a remarkable drop in the static birefringence was observed by Sirenko *et al.*[12] in (001) $(GaAs)_p/(AlAs)_p$ SL's, when the so-called SL period p is small ($p<14$). For larger periods, the measured birefringence reaches a plateau, whose height can be easily related to the classical birefringence predicted by the effective medium theory.[13–15] In fact, both quantum confinement and tunneling effects, which affect the carriers, vanish when the barrier and well widths become large enough with respect to the lattice constant. This justifies a simplified description of the medium as an arrangement of classical bulk dielectrics. In this limiting case, the dielectric constant tensor is obtained by the classical expression for a series and parallel arrangement of capacitors:[13]

$$\varepsilon_\perp = \langle \varepsilon \rangle = \frac{1}{2}(\varepsilon_{\mathrm{GaAs}} + \varepsilon_{\mathrm{AlAs}}), \tag{1}$$

$$\varepsilon_\parallel^{-1} = \langle \varepsilon^{-1} \rangle = \frac{1}{2}(\varepsilon_{\mathrm{GaAs}}^{-1} + \varepsilon_{\mathrm{AlAs}}^{-1}), \tag{2}$$

where $\varepsilon_{\mathrm{GaAs}}$ and $\varepsilon_{\mathrm{AlAs}}$ are the macroscopic dielectric constants of bulk GaAs and bulk AlAs, respectively.

Apart from this simple situation, the theoretical problem of determining the macroscopic dielectric functions of small-sized heterostructures is quite complex. To obtain accurate spectroscopic properties, one has to determine the SL band structures and take properly into account confinement effects

and confinement-induced multivalley and multiband mixings all over the Brillouin zone. This can in principle be done using either *ab initio* or semiempirical band structure calculation methods. *Ab initio* density functional theory[16,17] (DFT) calculations benefit from a high degree of precision and from their predictive power, but are demanding from a computational point of view. Therefore, in recent decades many empirical methods were developed in order to study large-scale heterostructures.[18] From this point of view, *ab initio* and empirical calculations play a complementary role, and should be combined to attain a complete comprehension, at different size scales, of the electronic properties of complex heterostructures. Of course, this is true only if the semiempirical description is able to catch all the essential physical effects that contribute to the experimental results.

In this work we explore both the *ab initio* DFT and the semiempirical linear combination of bulk bands[19] (LCBB) approach. A comparison of *ab initio* and semiempirical results, together with available measurements, not only leads to further insight into the physics of semiconductor SL's, but also allows a discussion of the advantages and disadvantages of the two different computational approaches.

In recent years, the electronic structure of GaAs/AlAs SL's was studied by means of DFT only for very short-period superlattices.[6,20] Concerning the optical properties, it is possible to find in the literature a few *ab initio* calculations for ultrathin multilayers,[21] semiempirical LCBB calculations,[22] and empirical tight-binding calculations for larger-scale systems.[5] All of these calculations are based on Fermi's golden rule, in terms of independent transitions between one-electron states. This approximation ignores contributions stemming from many-body effects. In particular, crystal local field effects (LFE's), which reflect the charge inhomogeneity of the responding medium, give sizable contributions in multilayer structures. Moreover, self-energy corrections and the electron-hole interaction are expected to be important, as they are known to modify significantly the line shape and the peak positions of GaAs and AlAs absorption spectra.[23,24]

Our recent calculations[25] of the SL dielectric constants $\varepsilon_{\parallel,\perp}(\omega=0)$ as a function of the SL period p, based on DFT and including LFE's, proved that, for any SL period, the qualitative behavior of the dielectric anisotropy is essentially governed by the interplay between quantum confinement and LFE's. In the present work we explain these results in more detail, and we complete them with additional findings (semiempirical and DFT band structures, dielectric constants obtained in different approximation schemes). Moreover, we show results for the absorption spectra obtained within time-dependent DFT (TDDFT),[26,27] including the strong continuum excitonic effect through the use of an appropriate model exchange-correlation (XC) kernel.[28] Finally, we pay particular attention to the description of the different terms contributing to the anisotropy of the dielectric response, by means of simple models. This allows us to give a consistent picture explaining when and why semiempirical or classical approximations and approximate descriptions of many-body effects can be used, as well as the possible sources of error in the calculations.

Concerning what follows, we briefly review the two approaches for the calculation of band structures in Sec. II and the theory of dielectric function calculations in Sec. IV. Then, we present our results for GaAs/AlAs SL's for different barrier and well widths: the electronic band structure (Sec. III), the frequency-dependent absorption spectra (Sec. V) and the static dielectric properties (Sec. VI). Finally, all results are summarized in Sec. VII.

TABLE I. Pseudopotential construction: reference configurations, core radii in bohrs, and generation scheme [H=Hamann scheme (Ref. 30), TM=Troullier and Martins scheme (Ref. 31)]. Nonlinear core-valence corrections are included for Ga and Al pseudopotentials (cutoff radius $r_{\mathrm{nlc}}=1.5$ bohr). The component chosen as local reference component is $l=0$ for all the atoms (Ref. 31).

Element	Reference configuration	l	r_l	Scheme
Ga	$4s^{1.5}4p^{0.5}4d^{0.5}$	0	1.20	H
	$4s^{1.5}4p^{0.5}4d^{0.5}$	1	1.25	H
	$4s^{1.5}4p^{0.5}4d^{0.5}$	2	1.45	H
Al	$3s^{2.0}3p^{1.0}3d^{0.0}$	0	1.93	TM
	$3s^{2.0}3p^{1.0}3d^{0.0}$	1	2.39	TM
	$3s^{0.75}3p^{1.0}3d^{0.25}$	2	2.52	TM
As	$4s^{2.0}4p^{3.0}4d^{0.0}$	0	1.15	H
	$4s^{2.0}4p^{3.0}4d^{0.0}$	2	1.60	H

II. TECHNICAL ASPECTS OF THE BAND STRUCTURE CALCULATIONS

We considered $(\mathrm{GaAs})_p/(\mathrm{AlAs})_p$ SL's, grown along the [001] crystallographic axis, with a barrier-well period p varying from 1 to 14. It is well known[29] that a structural relaxation of the supercell geometry is not necessary for GaAs/AlAs-based heterostructures, since the small lattice-constant mismatch ($\simeq 0.15\%$) makes negligible stress and strain effects at the interfaces. Assuming abrupt interfaces, the Bravais lattice is simple tetragonal, with a supercell defined by the basis vectors $(1,1,0)\ \langle a\rangle/2$, $(-1,1,0)\ \langle a\rangle/2$, $(0,0,p)\ \langle a\rangle$, where $\langle a\rangle$ is the average bulk lattice constant and p is the SL period.

The SL one-electron energy levels and wave functions were calculated using *ab initio* DFT (Refs. 16 and 17) and the semiempirical LCBB method (Ref. 19). We performed band structure calculations within DFT in the local density approximation (LDA),[17] using separable first-principles norm-conserving pseudopotentials and a plane wave expansion of the Kohn-Sham orbitals. We used for the LDA XC functional the parametrization of Perdew and Zunger[32] of the Monte Carlo results of Ceperley and Alder.[33] The atomic pseudopotentials were generated with the FHI98PP code.[34] The parameters used are listed in Table I. We tested various atomic pseudopotentials,[30,31] paying particular attention to the choice of the reference configurations: this is essential to reproduce the fact that the lattice mismatch between GaAs and AlAs is very small.[35] Furthermore, we found a strong improvement of the excitation properties of Ga and Al atoms when nonlinear core-valence corrections[36] are included. The same corrections turn out not to be relevant for the As

pseudopotential. The 3*d* semicore states of the Ga atom are slightly polarizable. This leads to errors of a few mRy in the atomic excitations, if the 3*d* states are treated as core states in the pseudopotential. This, however, does not justify the additional computational load which would follow from the inclusion of *d* states in the valence. The reliability of our atomic pseudopotentials was further confirmed by inspection of the structural properties and the optical spectra of GaAs and AlAs bulk crystals. In our self-consistent DFT calculations the plane wave cutoff energy was fixed at 35 Ry, independently of the SL period p. Integrations over the irreducible wedge of the Brillouin zone were evaluated using equivalent sets of **k** points for different supercell sizes. We performed extensive tests with respect to the number of **k** points and the size of the plane wave basis, in order to guarantee convergence to a few meV, for both the total energy and the eigenvalues. The bulk GaAs and AlAs lattice constants converged, respectively, to 10.59 and 10.61 a.u. (bohr). As usual in LDA calculations, these values are slightly smaller than the experimental ones, respectively, 10.69 and 10.70 bohr.[37] The theoretical estimation of the lattice mismatch is, however, in excellent agreement with the experimental value. Moreover, we found that the total energy of the SL does not change significantly when moving from the GaAs to the AlAs lattice constant and that the energy minimum is reached close to the intermediate value $\langle a \rangle = 10.60$. This value was used for the DFT calculations, while the average of the experimental lattice constants was used for the semiempirical calculations.

In Ref. 22 we adopted the LCBB method to determine the electronic states and the absorption spectra of GaAs/AlAs SL's. For all technical details and convergence tests we refer to that work. In the LCBB method, the heterostructure wave functions $\psi^{\mathrm{SL}}_{\mathbf{k}_{\mathrm{SL}},j}$ are expressed as linear combinations (over band indices i and wave vectors **k**) of full-zone Bloch eigenstates $\psi^{\sigma}_{\mathbf{k},i}$ of the constituent bulk materials:

$$\psi^{\mathrm{SL}}_{\mathbf{k}_{\mathrm{SL}},j}(\mathbf{r}) = \sum_{\sigma} \sum_{\mathbf{k},i}^{n_k,n_b} c^{(\mathbf{k}_{\mathrm{SL}},j)}_{\mathbf{k},i,\sigma} \psi^{\sigma}_{\mathbf{k},i}(\mathbf{r}), \tag{3}$$

where σ labels the bulk type (GaAs or AlAs), $\mathbf{k}_{\mathrm{SL}}$ is a wave vector inside the SL Brillouin zone (see Fig. 1), and j is the SL band index. Due to the supercell periodicity, the confining potential mixes only the $n_k = 2p$ bulk states labeled by **k** vectors which differ from $\mathbf{k}_{\mathrm{SL}}$ by a SL reciprocal lattice vector. This property allows us to use a small basis set, namely, $2p \times n_b$ bulk states, where n_b is the number of selected band indices. In the following we set n_b equal to 20. The total potential term in the SL Hamiltonian is a sum of screened, local, semiempirical atomic pseudopotentials v_α:

$$V(\mathbf{r}) = \sum_{\alpha} \sum_{\mathbf{d}_\alpha} \sum_{\mathbf{R}\in\mathbf{DL}} \mathbf{v}_\alpha(\mathbf{r} - \mathbf{R} - \mathbf{d}_\alpha), \tag{4}$$

where **R** is the tetragonal SL direct lattice (DL) vector and $\mathbf{d}_\alpha$ the displacement of the atom of type α in the primitive supercell. We employed the parametrized pseudopotential functions developed by Mäder and Zunger,[38] designed for a kinetic-energy cutoff of 5 Ry. The pseudopotential function $v_\alpha(\mathbf{q})$ is adjusted to reproduce the measured electronic properties of bulk GaAs and AlAs, and the DFT-LDA wave functions calculated for the ordered AlGaAs alloy (i.e., the monolayer SL). In semiempirical calculations, the fitting procedure entails implicitly the relativistic and many-body effects which can be described through a one-body local potential. This, in particular, allows us to circumvent the so-called gap problem present in DFT-LDA calculations of semiconductors.[39] In the heterostructure, As appears in three different environments, namely, surrounded by four Ga atoms, by four Al atoms, or by two Al and two Ga atoms. In this last situation, we use for the As pseudopotential the average of the pseudopotentials used in the two former situations. This choice preserves the symmetry of the crystal at the interface. The same pseudopotentials were employed to determine the bulk states, expanded on a plane wave basis.

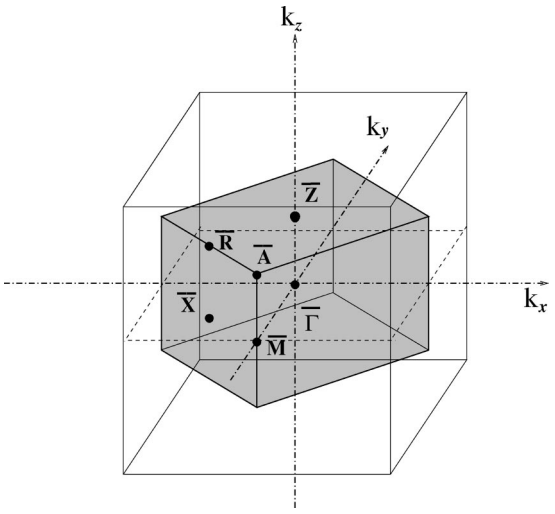

FIG. 1. Brillouin zone for simple tetragonal $(\mathrm{GaAs})_p/(\mathrm{AlAs})_p$ (001) SL's, included in bulk conventional cubic cell. High-symmetry points are shown.

The computational cost of the *ab initio* and semiempirical approaches is of course very different, starting from the number of plane waves N_{PW}. For comparison, we can consider the calculation of the band structure for a $p = 10$ SL. More than 20 000 plane waves are needed for the DFT calculations, whereas $N_{\mathrm{PW}} = 1200$ in the semiempirical approach. The CPU time required for the calculation of the bandstructure differs in this case by almost two orders of magnitude, and the random access memory requirement by one order of magnitude.

III. BAND STRUCTURES: RESULTS

Let us first look at the SL band structures along the high-symmetry directions in the tetragonal Brillouin zone (see Fig. 1), obtained within DFT-LDA. The dispersion of both the valence and the conduction bands is quite well described in bulk GaAs and AlAs (with an error bar of 0.1–0.2 eV).[39] Nevertheless, the energy gap is, as usual in LDA calculations,[39] largely underestimated. Additional self-energy corrections have essentially the effect of shifting rigidly upward the conduction bands by 0.8 eV for bulk GaAs and 0.9 eV for bulk AlAs, respectively ("scissor operator ap-

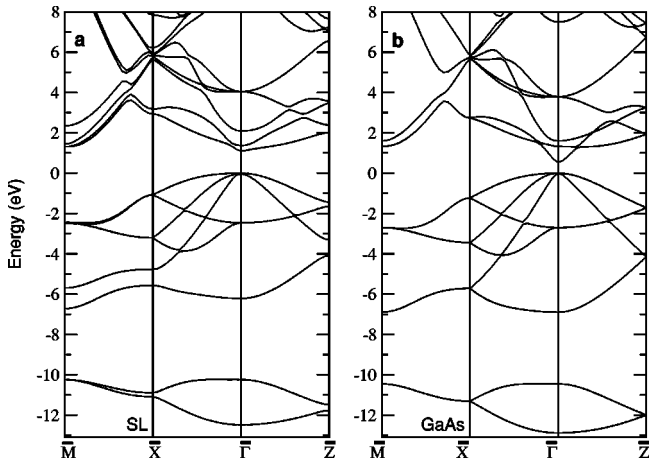

FIG. 2. Comparison between the Kohn-Sham LDA scalar-relativistic band structures of $(GaAs)_1/(AlAs)_1$ (a) and $(GaAs)_2$ (b) along high-symmetry directions. The energy zero is taken at the valence band maximum.

proximation"). Some authors have applied a similar "scissor operator" to very thin GaAs/AlAs SL's,[6] taking as reference quasiparticle calculations for the band energies of $p=1,2$ SL's.[20] We compared their DFT-LDA eigenvalues at the high-symmetry points for $p=1,2,3$ with our corresponding energy levels and found differences that never exceeded 0.1 eV. It should be noted that the Kohn-Sham eigenvalues do not have a direct physical interpretation. However, these eigenvalues, together with the Kohn-Sham eigenfunctions, can be used within TDDFT to obtain the optical properties and static dielectric constants. It is therefore instructive to analyze the evolution of the band dispersions and the Kohn-Sham gaps as a function of p over a large period range ($1 \leqslant p \leqslant 10$), and to compare DFT-LDA with semiempirical[22] LCBB band structures.

By comparing the $(GaAs)_p/(AlAs)_p$ SL band structure to the band structure of the material composing the layers where both electrons and holes are confined (i.e., GaAs), one can extract information about the magnitude of the confinement effects, which increase the gap, and of the confinement-induced tunneling and intervalley mixing, which displace energy levels and remove level degeneracies. In Fig. 2 we display the DFT-LDA band structures of $(GaAs)_1/(AlAs)_1$ and of its bulk counterpart $(GaAs)_2$. The latter was obtained by folding the bulk bands in the tetragonal Brillouin zone, in order to allow a direct comparison to the SL band dispersions. We observe a big increase of the SL direct gap (+80%) with respect to the GaAs gap. Furthermore, at $\bar{\Gamma}$, $\bar{Z}$, and $\bar{M}$ the threefold degeneracies are always removed. As the spin-orbit interaction is not included, at the point $\bar{\Gamma}$ we obtain a twofold degenerate "heavy hole" and a single "light hole" state.[40] The large bandwidths along the $\bar{\Gamma}$-$\bar{Z}$ direction are the consequence of strong electron tunneling, resulting from the thin barrier widths. For $p=1$, the DFT-LDA band structure shows an indirect gap, as the conduction band minimum is found at $\bar{R}$. This is in agreement with quasiparticle calculations,[20] but in disagreement with experimental luminescence data, which place the conduction

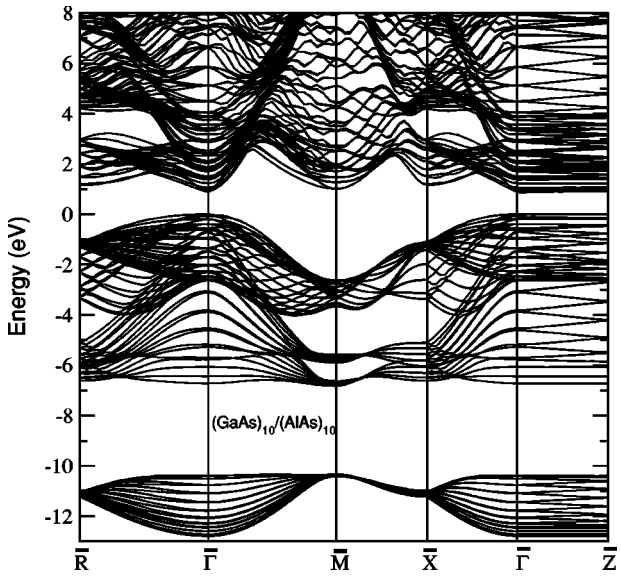

FIG. 3. Kohn-Sham LDA scalar-relativistic band structure of a $(GAAs)_{10}/(AlAs)_{10}$ (001) SL along the high-symmetry directions. The energy zero is taken at the valence band maximum.

minimum at $\bar{M}$.[41] For all other supercell sizes ($p \geqslant 2$)), our DFT-LDA gap is a direct gap at the $\bar{\Gamma}$ point. Quasiparticle calculations[20] cannot reveal the nature of the gap for $p=2$, since the $\bar{M}$ and $\bar{\Gamma}$ states are too close in energy. Luminescence data[41] show that the indirect character of the gap (conduction minimum in $\bar{M}$) is conserved up to $p=3$. Then, starting from $p=4$, the conduction minimum is located at $\bar{\Gamma}$.[42]

The ordered alloy for $p=1$ (and to a smaller extent also the $p=2$ SL) possesses very peculiar properties, that cannot be deduced from the general behavior of GaAs/AlAs multilayers as a function of the SL period. However, general trends can be easily established for $p \geqslant 3$ SL's. When p increases, tunneling and confinement quantum effects vanish progressively. It is then possible to have a classical description in terms of the electronic properties of the bulk constituents.

In Fig. 3 we reproduce the DFT-LDA band structure of a $(GaAs)_{10}/(AlAs)_{10}$ (001) SL, which can be directly compared to the LCBB band structure for the same SL reported in Fig. 4 of Ref. 22. The band folding makes the SL band structure highly dense for $p=10$; thus the dispersion of a single band cannot be detected by a simple inspection of the figure. However, we verified carefully that the *ab initio* and semiempirical band dispersions and widths are similar, for both the valence and conduction states. In fact, for all SL periods considered, if the conduction DFT-LDA bands are shifted rigidly upward to compensate for the underestimation of the band gap in the Kohn-Sham scheme, the DFT-LDA and LCBB bands coincide. This agreement is better for the lowest conduction levels, up to 10 eV. Similarly to bulk GaAs calculations, the DFT-LDA SL gap is about 50–60 % smaller than the corresponding semiempirical gap. The larger semiempirical gap is of course caused by the semiempirical fitting procedure based on the experimental optical spectra. A systematic study of the evolution of the band gap at Γ as a

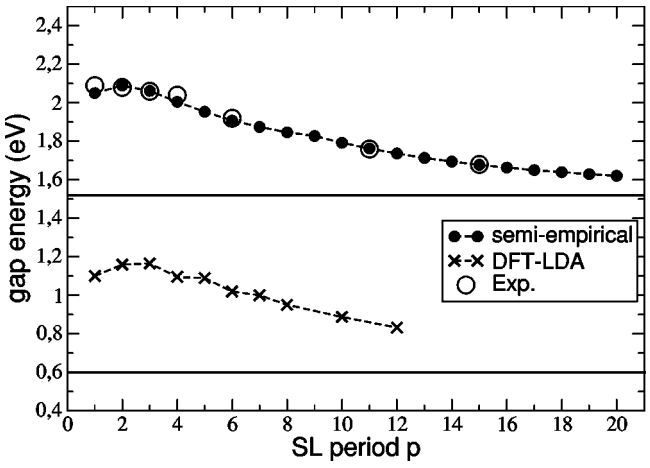

FIG. 4. Photoemission gaps for $(GaAs)_p/(AlAs)_p$ SL's as a function of the SL period p, calculated by the LCBB method (filled circles) and as the difference of Kohn-Sham LDA eigenvalues (crosses). The horizontal lines represent the gap energies in GaAs bulk, obtained by LCBB and DFT-LDA. The open circles are the experimental data (Ref. 43).

function of p is presented in Fig. 4 (the experimental data are shown as well[43]). Despite the difference in the absolute value of the gap energy, we find exactly the same slope in the semiempirical and DFT-LDA curves: for $p \geqslant 3$ the gap energy starts to decrease toward the respective (i.e., experimental or DFT-LDA) GaAs Γ gap values. As expected, the semiempirical results are very close to the measured ones.

Sizable differences between semiempirical and DFT-LDA band dispersions cannot be easily detected, even for small period SL's. Nevertheless, we will see in Sec. VI that the semiempirical and *ab initio* dielectric tensors differ drastically for small p. The reason for this fact is that the discrepancies between the calculated wave functions turn out to be more pronounced and more important than the discrepancies in the energy bands, especially close to the interfaces. This statement is illustrated in Fig. 5, where we can see the normalized electron density profiles $\rho(z)$, averaged in the plane, along the SL growth direction z. The upper panel of Fig. 5 shows the results of the DFT-LDA calculations: we can observe that the SL electron density (continuous line) is similar to the bulk GaAs electron density (dashed line) inside the GaAs layer and to the bulk AlAs electron density (dotted line) inside the AlAs layer. In the region around the As layer which is located at the interface, the SL density has an intermediate value between GaAs and AlAs densities. The lower panel of Fig. 5 shows the results of LCBB calculations: the SL density is essentially still close to the bulk densities inside the layers, but at the As interface there is an abrupt change of the SL density from GaAs-like to AlAs-like. This behavior can be traced back to the symmetrization of the As pseudopotential for the As atoms at the interface.

In conclusion, in the DFT-LDA calculations, the perturbation due to the presence of a mixed Ga-As-Al bond propagates inside the GaAs (or AlAs) layer, which makes the interface less abrupt than in LCBB. We will discuss in Sec. VI how this effect can affect the anisotropy of the dielectric response in the small barrier and well width range, where the relative weight of interfaces is more important.

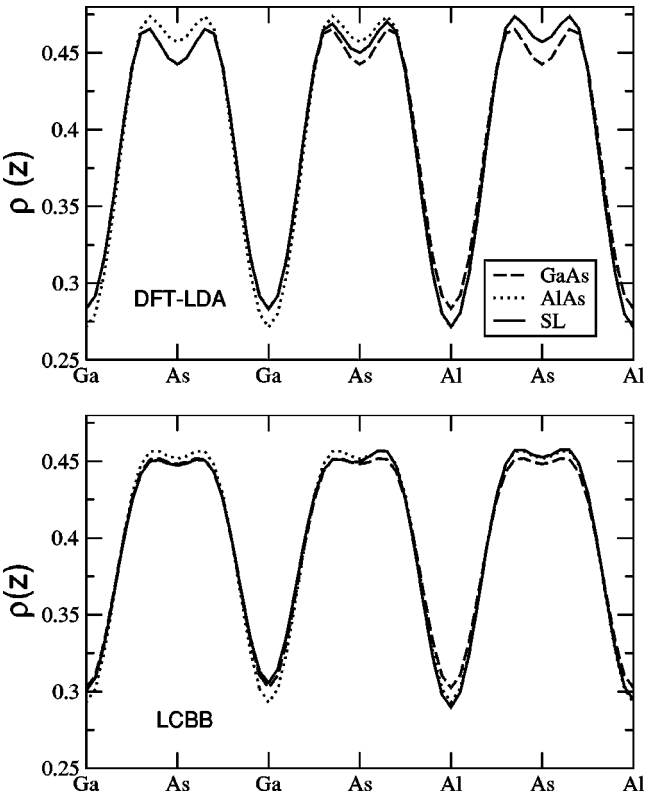

FIG. 5. Averaged in-plane electron density along the tetragonal z axis for bulk GaAs (dashed line), bulk AlAs (dotted line), and $(GaAs)_3/(AlAs)_3$ (solid line). Upper panel: DFT-LDA calculations. Lower panel: semiempirical LCBB calculations.

IV. THE MACROSCOPIC DIELECTRIC TENSOR: THEORY

We now proceed to the calculation of the SL optical properties.

The electronic states all over the Brillouin zone, obtained either by the DFT-LDA or by the LCBB method, are the main ingredient for the calculation of the microscopic dielectric function $\varepsilon(\mathbf{r},\mathbf{r}';\omega)$. For periodic systems, a formulation in the reciprocal space is often convenient: the Fourier transform of $\varepsilon(\mathbf{r},\mathbf{r}';\omega)$ is a $\mathbf{G}$, $\mathbf{G}'$ matrix (where the $\mathbf{G}$'s are reciprocal lattice vectors), which depends on a wave vector $\mathbf{q}$ belonging to the first Brillouin zone: $\varepsilon_{\mathbf{G},\mathbf{G}'}(\mathbf{q},\omega)$. An optical experiment measures the macroscopic response of the system. In the long wavelength limit ($\mathbf{q}\rightarrow\mathbf{0}$), an absorption spectrum is described by the imaginary part of the macroscopic dielectric function $\varepsilon_M(\omega)$. The electronic dielectric constant is the real part of $\varepsilon_M(\omega)$ at a frequency equal to zero. In a uniaxial system, $\varepsilon_{\mathbf{G},\mathbf{G}'}(\mathbf{q},\omega)$ depends on the direction of the wave vector $\mathbf{q}$. Consequently, the dielectric function is not a scalar quantity, but a diagonal tensor, defined by two distinct elements $\varepsilon_{\parallel}=\varepsilon_{zz}$ and $\varepsilon_{\perp}=\varepsilon_{xx}=\varepsilon_{yy}$, where the z axis is taken along the growth direction. As we are looking at absorption spectra, and for the periods of the SL's we considered, we do not have any additional symmetry breaking

problem due to the finite value of $\mathbf{q}$, as described, e.g., in Ref. 44.

In this work we adopt an approach based on time-dependent DFT. We start from the expression for the macroscopic dielectric response, which reads[45,46]

$$\varepsilon_M(\omega) = \lim_{\mathbf{q}\to\mathbf{0}} \frac{1}{\varepsilon^{-1}_{\mathbf{G}=\mathbf{G}'=\mathbf{0}}(\mathbf{q},\omega)}. \quad (5)$$

When an external macroscopic field is applied, induced microscopic ($\mathbf{G},\mathbf{G}' \neq 0$) variations appear in the response of the medium, contributing to ε_M. The contributions due to the presence of the $\mathbf{G}\mathbf{G}'$ off-diagonal elements of $\varepsilon_{\mathbf{G},\mathbf{G}'}$ are the crystal local field effects. They vanish for a homogeneous medium, where Eq. (5) reduces to

$$\varepsilon_M(\omega) = \lim_{\mathbf{q}\to\mathbf{0}} \varepsilon_{\mathbf{G}=\mathbf{G}'=\mathbf{0}}(\mathbf{q},\omega). \quad (6)$$

The matrix inversion in Eq. (5) mixes formerly independent transitions, even in the random phase approximation (RPA); it can therefore drastically change ε_M due to interference effects. Not only $\varepsilon_{\mathbf{00}}(\mathbf{q},\omega)$ but also the LFE's depend on the direction of $\mathbf{q}$, and thus contribute to the anisotropy of the response. These facts will be important below for the interpretation of our results, to show that the anisotropy of the dielectric tensor in the static limit is governed by the anisotropy of the LFE's.

To identify the different contributions to the dielectric response, it is useful to write the macroscopic dielectric function as

$$\varepsilon_M(\omega) = \lim_{\mathbf{q}\to\mathbf{0}} [1 - v_{\mathbf{G}=\mathbf{0}}(\mathbf{q})\overline{\chi}(\mathbf{q},\mathbf{G}=\mathbf{0},\mathbf{G}'=\mathbf{0},\omega)], \quad (7)$$

where $v_{\mathbf{G}=\mathbf{0}}$ is the Fourier transform of the bare Coulomb interaction. In TDDFT, the modified response function $\overline{\chi}$ obeys the matrix equation

$$\overline{\chi} = \chi_0 + \chi_0(\overline{v} + f_{\mathrm{XC}})\overline{\chi}. \quad (8)$$

The independent-particle polarizability χ_0, after a summation over the spin, can be constructed from the *ab initio* or semiempirical wave functions ϕ_i, eigenvalues ε_i, and occupation numbers f_i:

$$\chi_0(\mathbf{r},\mathbf{r}',\omega) = 2\sum_{i,j} (f_i - f_j) \frac{\phi_i(\mathbf{r})\phi_j^*(\mathbf{r})\phi_i^*(\mathbf{r}')\phi_j(\mathbf{r}')}{\epsilon_i - \epsilon_j - \omega - i\eta}. \quad (9)$$

$\overline{v}$ is a modified Coulomb interaction: $\overline{v}_{\mathbf{G}}(\mathbf{q})$ is $v_{\mathbf{G}}(\mathbf{q})$ for all $\mathbf{G}$, except for the long-range term $v_{\mathbf{G}=\mathbf{0}}(\mathbf{q})$ which is set to zero. $\overline{v}$ is in fact the microscopic part of the variation of the Hartree potential with respect to the density. Its inclusion is equivalent to the inclusion of LFE's. f_{XC} is the XC kernel, defined as the functional derivative of the time-dependent XC potential with respect to the density; it is in principle ω dependent. As its exact form is unknown, we have to use some approximated expressions.

In the RPA, f_{XC} is set to zero, hence XC terms are completely neglected. The adiabatic local density approximation (TDLDA) consists in writing f_{XC} as the functional derivative with respect to the density of the adiabatic LDA XC potential evaluated at the ground state density. It is well known that the RPA can give large discrepancies between calculated and measured spectra, and this is the case for GaAs and AlAs bulk crystals. It is also known that the TDLDA does not improve significantly the quality of absorption spectra or dielectric constants in extended systems. To calculate improved SL spectra, we will apply instead a static long-range XC kernel, proposed by Reining *et al.*[28] and further tested by Botti *et al.*:[24] it has been shown that a *static* long-range contribution (LRC) of the form

$$f_{\mathrm{XC}}^{\mathrm{LRC}}(\mathbf{q},\mathbf{G},\mathbf{G}',\omega) = -\delta_{\mathbf{G},\mathbf{G}'}\alpha/|\mathbf{q}+\mathbf{G}|^2, \quad (10)$$

where α is a static material-dependent parameter that is inversely proportional to the dielectric constant,[24] can simulate the strong continuum excitonic effect in the absorption spectrum of bulk semiconductors, provided that quasiparticle eigenvalues are used instead of Kohn-Sham LDA eigenvalues in the construction of $\chi_0 = \chi_0^{\mathrm{QP}}$. As is further discussed in Ref. 24, this approximation drastically improves the absorption spectra of bulk GaAs and AlAs.[24] In order to make the link to our earlier work,[25] we note that from Eqs. (7) and (8) (with $\chi_0 = \chi_0^{\mathrm{QP}}$) one can extract[47]

$$\varepsilon_M(\omega) = 1 + \frac{\varepsilon_M^{\mathrm{QP\text{-}RPA}}(\omega) - 1}{1 + g(\omega)[\varepsilon_M^{\mathrm{QP\text{-}RPA}}(\omega) - 1]} \quad (11)$$

where $g(\omega) = \lim_{\mathbf{q}\to\mathbf{0}} q^2 f_{\mathrm{XC}}(\mathbf{q},\omega)/4\pi$ and $\varepsilon_M^{\mathrm{QP\text{-}RPA}}$ is the macroscopic dielectric function obtained in the RPA, after the inclusion of quasiparticle corrections to the Kohn-Sham energy eigenvalues. As pointed out in Ref. 47, Eq. (11) is equivalent to the contact exciton approximation.[48] When the LRC approximation is used for f_{XC} the contact exciton parameter $g(\omega)$ corresponds to $-\alpha/4\pi$, where α is the parameter weighting $1/q^2$ in the XC kernel. In fact, in Ref. 25 we have already used the contact exciton model via the expression (11), to include excitonic corrections in the calculation of the static birefringence. This contribution turned out to be essential to reach a quantitative agreement with the experimental plateau value, although the qualitative dependence of the birefringence on p was determined by the anisotropy of the LFE's. Results for the static birefringence Δn as a function of the SL period have been presented in Fig. 2 of Ref. 25 and are not repeated here, whereas we will show optical spectra obtained using the LRC approach.

Independently of the question if (11) is considered as a contact exciton, or as an approximate TDDFT approach, the difference from the original work[24,28,47,48] lies in the fact that here we consider an anisotropic material, which leads us to consider the possibility of using two different parameters α for the two light polarizations. Below, in Sec. V, we will explain how we get these parameters.

Finally, it is also possible to neglect both XC contributions ($f_{\mathrm{XC}}=0$) and LFE's ($\overline{v}=0$). In that case the evaluation of absorption reduces to the naive independent-particle transition picture of Fermi's golden rule:

$$\varepsilon_M(\omega) = \lim_{\mathbf{q}\to\mathbf{0}} \varepsilon_{00}(\mathbf{q},\omega) = \lim_{\mathbf{q}\to\mathbf{0}} [1 - v_{\mathbf{0}}(\mathbf{q})\chi_0(\mathbf{q},\mathbf{G}=\mathbf{0},\mathbf{G}'=\mathbf{0},\omega)]. \tag{12}$$

In the application of TDDFT to SL systems, we will discuss different levels of approximation to account for crystal LFE's and XC terms.

V. ABSORPTION SPECTRA

The quality of the the spectra obtained in TDDFT is limited by the quality of the approximate expressions for the unknown XC potential v_{XC} and, especially, for the XC kernel f_{XC}. We performed *ab initio* TDDFT calculations for the absorption spectra of $p=1,3,6$, $(GaAs)_p/(AlAs)_p$ (001) SL's, by averaging over the direction of light polarization. We employed various approximations: the RPA based on a DFT-LDA band structure (including and neglecting LFE's), the TDLDA, and the long-range XC kernel f_{XC}^{LRC} defined above. Since the last approach gave excellent results for GaAs and AlAs bulk spectra,[24] we expect it to be able to give a good description also of the heterostructures composed of these two constituents. This formulation requires the quasiparticle eigenvalues; we have thus applied a scissor operator of 0.85 eV, which is the intermediate value between the calculated scissor operators of 0.8 eV, for GaAs and 0.9 eV for AlAs.[39] The value chosen for the scissor approximation is confirmed to be reasonable by inspection of the gap values in Fig. 4: the semiempirical gaps reproduce the quasiparticle gap and are larger than Kohn-Sham DFT gaps by about 0.85–0.9 eV for all considered periods.

We have discussed above that a SL is a uniaxial system, where the optical response is dependent on the direction of the $\mathbf{q}$ vector. The XC kernel $f_{XC}(\mathbf{q},\mathbf{G},\mathbf{G}',\omega)$ depends on $\mathbf{q}$ as well; thus we introduced two different parameters $\alpha_\parallel$ and $\alpha_\perp$ corresponding, respectively, to $\mathbf{q}$ along the z axis or in the plane perpendicular to it. The values of the parameters were fixed by exploiting their linear dependence on the inverse of the dielectric constant. We can in fact use the curve of α versus ε^{-1} in Ref. 24, which was obtained by interpolating the values of α for a variety of semiconductor crystals:

$$\alpha_{\parallel,\perp} = 4.615\varepsilon_{\parallel,\perp}^{-1} - 0.213. \tag{13}$$

The absorption spectra are in general rather stable with respect to small changes in α. The slight difference between in-plane and in-growth components of the SL dielectric constants affects the value of α by less than 5%. Since we are not considering the anisotropy of the absorption spectrum, in this section we could take the same value $\alpha=0.3$ for $\alpha_\parallel$ and $\alpha_\perp$. Moreover, as the dielectric constant does not change too much in going from $p=1$ to $p=6$ we could select the same value $\alpha=0.3$ for all the SL's considered.[49]

In Fig. 6 we present as an example the calculated and experimental absorption spectra for the $(GaAs)_3/(AlAs)_3$ SL. The dots are the experimental data from Ref. 1. The dot-dashed curve stems from a standard TDLDA calculation (i.e., using DFT-LDA eigenvalues and applying the static LDA XC kernel). The well-known discrepancies with experiment are evident: the peak positions are wrong (the spectrum exhibits a redshift), and the intensity of the first peak (the E_1 peak) is strongly underestimated. A very similar result is obtained within the RPA (not shown in Fig. 6). The dashed curve is calculated by replacing the Kohn-Sham eigenvalues with quasiparticle (scissor operator) energies in the RPA expression of ε. The resulting spectrum is excessively blueshifted and, additionally, the height of the E_1 structure has not been corrected. The continuous curve represents the calculation which contains the long-range contribution f_{XC}^{LRC} (TDDFT-LRC) to the XC kernel: both the peak positions and the intensities are substantially modified, and are closer to the experimental curve. The sole measurements found in the literature[1] were obtained at room temperature, while our calculations were performed at zero temperature. This fact, together with the approximations discussed above, explains why the agreement between calculated and experimental curves for SL's is not as good as for GaAs and AlAs bulk systems. Nevertheless, the improvement with respect to standard TDLDA calculations is undoubtable, with the advantage of not requiring any additional numerical cost and, thanks to the use of Eq. (13), without using any empirical fit parameter.

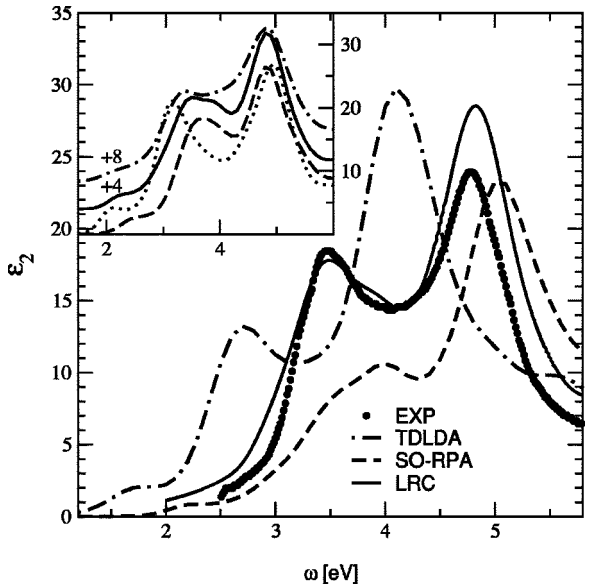

FIG. 6. Imaginary part of the dielectric function of a $(GaAs)_3/(AlAs)_3$ SL from *ab initio* calculations. Dots: experimental results (Ref. 1). Dot-dashed curve: TDLDA. Dashed curve: RPA using the scissor operator. Continuous curve: TDDFT-LRC. In the inset the TDDFT-LRC curve for $p=3$ (continuous line, shifted upward by +4) is represented together with the LRC curves for $p=1$ (dashed line) and $p=6$ (dot-dashed line, shifted upward by +8). The TDDFT-LRC calculation for bulk GaAs (dotted line) is shown as well (Ref. 43).

In the inset of Fig. 6, we compare the TDDFT-LRC curves for different SL periods, $p=1$ (dashed line), $p=3$ (continuous line), $p=6$ (dot-dashed line). The GaAs absorption spectrum is shown as well (dotted line): we remark the expected redshift of the E_1 peak as the period increases, as a consequence of the weakening of confinement effects. The second structure (the E_2 peak) comes from transitions between weakly confined states and is thus stable at 4.8 eV.

These results confirm the qualitative conclusions based on analogous LCBB spectra, presented in Ref. 22.

VI. DIELECTRIC CONSTANT AND BIREFRINGENCE

The birefringence Δn, defined as the difference in the refractive index components $\Delta n = \sqrt{\varepsilon_\perp} - \sqrt{\varepsilon_\parallel}$, measures the dielectric anisotropy of a medium. Here we focus on the zero-frequency birefringence, whose peculiar behavior as a function of the layer thickness was measured in Ref. 12. For large periods, the experimental birefringence reaches a plateau value of $\simeq 0.3$, which agrees with the effective medium value obtained starting from the experimental dielectric constants[50] of GaAs and AlAs ($\varepsilon^{\text{expt}}_{\text{GaAs}} = 10.6$ and $\varepsilon^{\text{expt}}_{\text{AlAs}} = 8.2$). In order to shed light on these experimental findings, we presented in Refs. 22 and 25 both semiempirical and *ab initio* calculations within the RPA, including and neglecting LFE's, and (in Ref. 25) within TDDFT-LRC. Now we want to analyze these and further results in more detail, in order to clarify the role of different contributions to the anisotropy, in particular of LFE's.

Due to confinement in the z direction, the p-like top valence states at $\bar{\Gamma}$ split into a doubly degenerate heavy hole and a single light hole state.[40] As predicted by symmetry selection rules, at $\bar{\Gamma}$ the lowest conduction states are coupled to valence light hole states by light polarized along the growth direction, whereas the heavy hole states respond to light polarized in plane. Of course, this phenomenon is not restricted to the $\bar{\Gamma}$ point or to the levels close to the gap, and the order and character of the coupled states change throughout the Brillouin zone. This prevents the description of the birefringence by means of a simple analytical model.

To get a deeper insight into how the LFE's act on the birefringence, it is interesting to understand which transitions determine the anisotropy of the dielectric response. We explore this idea by examining the effect of adding groups of bands: we already discussed the contributions of the valence bands to the birefringence in Ref. 25; here we add the analysis of the conduction band contributions to the band sums in Eq. (9). The general behavior is the same for all SL periods studied. In Fig. 7 we show as an example the results obtained for the well-barrier periods $p=3$ and $p=8$ within the RPA. As a first step, as discussed in Ref. 25, we took into account "all" conduction bands (i.e., those necessary to achieve convergence) as possible final states for the transitions, but we restricted the initial states to the first v valence bands (Fig. 7, lower panel). In order to scale the results, the values on the x axis vary from lattice to lattice, with $v=ip$, i being an integer. We found that the lowest bands do not give rise to a sizable birefringence and that the large positive contribution arising from the bands $4p$ to $6p$ is almost completely canceled by the contribution from the (folded) light hole and heavy hole bands $6p$ to $8p$. In a second step, we considered all the occupied bands as possible initial states, and restricted the final states to a group of high conduction bands, starting from the cth band (Fig. 7, upper panel) to the last band included in converged calculations. In Fig. 7 the number of conduction bands is $c=(i-1)p+1$, where i has already been

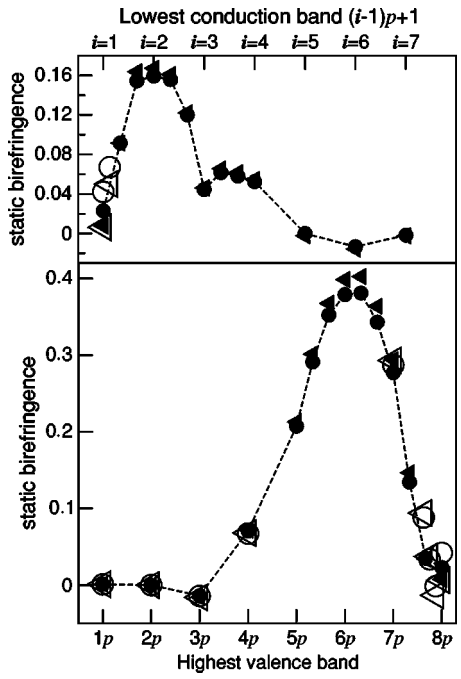

FIG. 7. Contribution to the birefringence of the valence bands (lower panel) and of the conduction bands (upper panel) for $p=3$ (filled symbols) and $p=8$ (empty symbols). Circles, contributions with LFE's triangles, contributions without LFE's. The dashed line is a guide to the eyes for the $p=3$ SL with LFE's.

defined. Once again, the transitions to the higher conduction bands do not contribute to the birefringence. The large contributions to birefringence of both conduction and valence bands are associated with p-like states. In fact, the level splittings which give rise to anisotropy in the absorption also yield a contribution to the static anisotropy, through the Kramers-Kronig relation

$$\text{Re}[\varepsilon_{\text{M}}(0)] = 1 + \frac{2}{\pi}\int_0^\infty \frac{\text{Im}[\varepsilon_{\text{M}}(\omega)]}{\omega} d\omega. \qquad (14)$$

Nevertheless, the large steplike positive contribution of the intermediate group of conduction and valence bands is compensated by the contribution of lowest (highest) conduction (valence) bands. Adding up either valence bands or conduction bands, if LFE's are neglected the cancellation is almost total. The contribution of LFE's to the birefringence can be measured from the difference between the circles and triangles in Fig. 7. We observe that this contribution changes sign upon the inclusion of the highest valence bands (or the lowest conduction bands), so it becomes positive (i.e., the static birefringence is larger when LFE's are included) and dominated by the anisotropy arising from transitions involving p-like states. The large cancellation effects are essential: it is thus important to evaluate the integral (14) over an adequate frequency range. For this reason, a description involving only transitions from the highest valence to the lowest conduction bands is inadequate and can lead to an estimated birefringence with the wrong sign and about a factor of 10 too large.

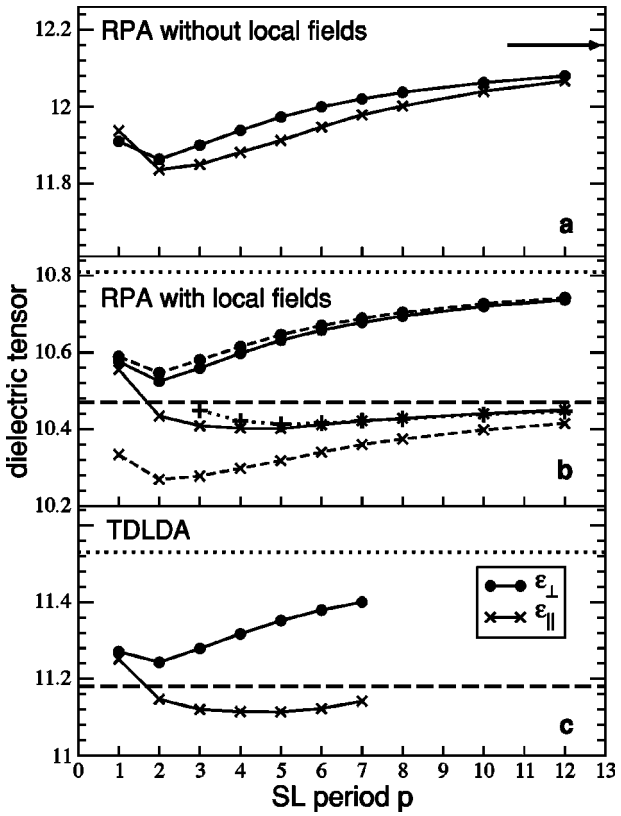

FIG. 8. Dielectric tensor components in-growth $\varepsilon_{\parallel}$ and in-plane $\varepsilon_{\perp}$ (continuous lines) as a function of the SL period p, calculated within the RPA neglecting LFE's (a), within the RPA including LFE's (b), and within the TDLDA (c). In panel (b), the dashed and dotted curves refer to the corresponding model calculations, as described in the text. The arrow in (a) marks the average of the bulk GaAs and AlAs dielectric constants, calculated without LFE's. Dotted (dashed) lines in (b) and (c): effective medium values of in-plane (in-growth) components.

Nevertheless, considering only the lifting of degeneracies and the associated selection rules can be sufficient to give an intuitive picture of the trend in the static dielectric tensor components as a function of the SL period, provided that LFE's are neglected in the calculations [see Fig. 8(a)]. In that case, the response of the medium can be interpreted in terms of a sum of independent transitions (Fermi's golden rule). Both the in-plane and the in-growth components get larger when the SL period increases. This fact is related to the decreasing of confinement effects for thicker layers, which produces smaller energy gaps. The selection rules discussed above explain why the in-growth component is always smaller than the in-plane one (except for the atypical $p=1$ ordered alloy): in fact, it corresponds to the polarization for which light experiences a larger gap. Furthermore, when the SL period increases, the confinement-induced splittings become smaller and the anisotropy of the response, i.e., the distance between the in-plane and in-growth curves, vanishes. When LFE's or even XC effects are taken into account, the interpretation of the calculated dielectric components becomes less intuitive [see in Figs. 8(b) and 8(c)]. χ_0 is still a sum over independent transitions; however, the relation between the macroscopic dielectric constant ε_M and χ_0 (even in the RPA) is much more complicated than the simple linear relation (12), which is used in calculations without LFE's. The extra term in Eq. (7), or equivalently the result of the matrix inversion in Eq. (5), is in fact sensitive to the direction of polarization of the light, through the dependence of the wing elements of $\varepsilon_{\mathbf{G},\mathbf{G}'}$ on the $\mathbf{q}$ vector. In Fig. 8(b) we can observe that, for the in-plane component, the consequence of the inclusion of LFE's is a rigid downward shift (by a quantity that equals the average shift of bulk GaAs and AlAs dielectric constants) of the dielectric constant components at any SL period. The in-growth components, on the other hand, contain LFE contributions which are negative in sign and increasingly large as the SL period grows; thus they have the tendency to balance the decreasing confinement effects, making the resulting $\varepsilon_{\parallel}$ always close to its classical effective medium value (dashed horizontal line) given in Eq. (2).

The inclusion of the XC contributions within the TDLDA (Refs. 26 and 27) significantly increases the dielectric constant components with respect to RPA calculations. This is also true for both constituent bulk semiconductors (+7% with respect to the RPA values, consistent with earlier results[35,51]). Despite these significant changes, the contributions completely cancel out in the birefringence, where the two components of the dielectric tensor are only rigidly shifted on moving from Fig. 8(b) to 8(c). This result is not surprising if we estimate roughly, applying the effective medium theory, the contribution to the large period static birefringence resulting from an increase by 7% of both constituent dielectric constants. It is given by $\Delta n^{\mathrm{TDLDA}}(p\to\infty) = \sqrt{1+\gamma}\Delta n^{\mathrm{RPA}}(p\to\infty)$, where $\gamma=0.07$ and Δn^{RPA} is the birefringence obtained using the RPA dielectric constants of GaAs and AlAs.

This means that the inclusion of XC terms within the TDLDA leads to a change of the RPA plateau of only a few percent. This is within the accuracy of the calculated birefringence. The complete cancellation of TDLDA effects in the birefringence occurs, however, only by chance, namely, because GaAs and AlAs exhibit a very similar XC correction. Therefore it cannot be considered to be a general feature. In fact, a sizable change in the birefringence can be expected in the case of different TDLDA corrections to the two bulk constituents; in that case the magnitude of the correction to the SL birefringence would depend also on the dielectric mismatch of the two constituents. To give an example, if the TDLDA correction to one of the two constituent (let us say AlAs) were 5% instead of 7%, the resulting correction to the birefringence would be 5 times larger.

In Fig. 9 we show the results of a semiempirical calculation of the static dielectric tensor components $\varepsilon_{\parallel}$ and $\varepsilon_{\perp}$, as a function of the SL period, neglecting (upper panel) and including (lower panel) LFE's. The LFE's $\varepsilon_{\parallel,\perp}^{\mathrm{LF}}-\varepsilon_{\parallel,\perp}^{\mathrm{NLF}}$ are displayed in the inset. We can observe that only when p is large enough are the trends of $\varepsilon_{\parallel}$ and $\varepsilon_{\perp}$ rather similar to the corresponding trends in *ab initio* calculations. For small barrier and well widths, instead, the behavior is quite different. Even without LFE's (Fig. 9, upper panel), the semiempirical calculation shows a larger anisotropy, which increases when the SL period decreases and which tends to zero more slowly in the large-p limit. When LFE's are included (Fig. 9, lower

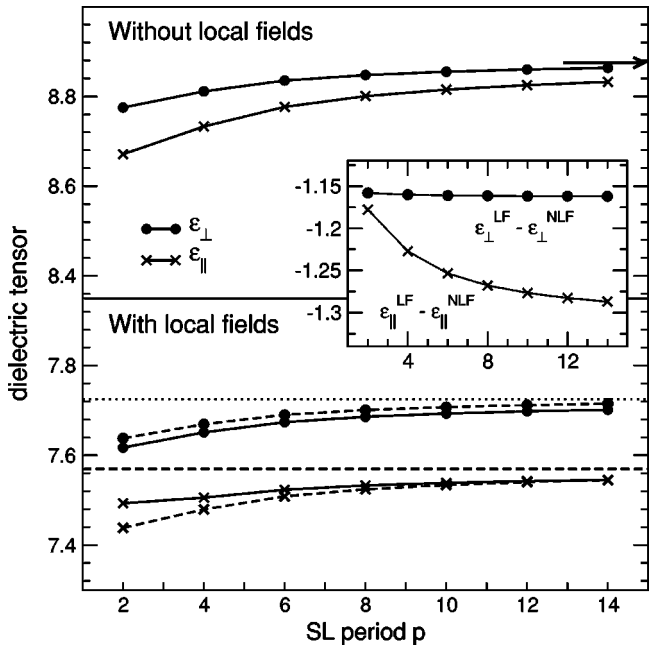

FIG. 9. Dielectric tensor components (continuous curves) calculated from the semiempirical electronic states without ($\varepsilon^{\mathrm{NLF}}$, upper panel) and with ($\varepsilon^{\mathrm{LF}}$, lower panel) LFE's, as a function of the SL period p. The dashed curves refer to the corresponding model calculations described in the text. Arrow: average of semiempirical bulk GaAs and AlAs dielectric constants, calculated without LFE's. Dotted (dashed) line: semiempirical effective medium value of $\varepsilon_{\perp}$ ($\varepsilon_{\parallel}$). In the inset we display the LFE's $\varepsilon^{\mathrm{LF}}_{\parallel,\perp}-\varepsilon^{\mathrm{NLF}}_{\parallel,\perp}$.

panel) the two curves for $\varepsilon_{\parallel}$ and $\varepsilon_{\perp}$ become almost parallel, in strong contrast to the *ab initio* results and the experiment. Later, we will see that in fact this result is due to the sharpness of interfaces in semiempirical calculations and that a smoother interface corrects this error.

However, the LFE dependence on p is very similar in the *ab initio* (see Fig. 1 in Ref. 25) and semiempirical (see inset in Fig. 9) approaches. First, LFE's are always negative, since they bring into play higher-energy transitions in the important gap region, which decrease the dielectric constants. Second, their dependence on the SL period is drastically different for the in-plane and in-growth polarization of light: the in-plane LFE's $\varepsilon^{\mathrm{LF}}_{\perp}-\varepsilon^{\mathrm{NLF}}_{\perp}$ show a very weak dependence on p, while in-growth LFE's increase in absolute value with increasing p. In the growth direction, the increase in magnitude of the LFE's with increasing p counterbalances the effects of quantum confinement on the independent-particle transitions, and leads, in the *ab initio* calculations, to a macroscopic dielectric constant $\varepsilon_{\parallel}$ close to its effective medium value at any period p. The anisotropy of LFE's allows us to approach for large p the finite classical limit value of the birefringence.

In order to explain the different effect of the LFE's in the two polarization directions, we apply a model based on simple physical observations: using the effective medium theory, we write the dielectric constant components without LFE's as a function of the bulk dielectric constants and a function y describing the confinement effects:

$$\varepsilon^{\mathrm{NLF}}_{\perp}=\frac{1}{2}[\varepsilon^{\mathrm{NLF}}_{\mathrm{GaAs}}y_{\perp}(p)+\varepsilon^{\mathrm{NLF}}_{\mathrm{AlAs}}], \tag{15}$$

$$\varepsilon^{\mathrm{NLF}}_{\parallel}=\frac{1}{2}[\varepsilon^{\mathrm{NLF}}_{\mathrm{GaAs}}y_{\parallel}(p)+\varepsilon^{\mathrm{NLF}}_{\mathrm{AlAs}}]. \tag{16}$$

Here the assumption is the following. In Eqs. (15) and (16) the functions $y_{\perp,\parallel}(p)$ account for the change in the effective dielectric constant of the GaAs layer, due to the confinement of carriers in this region. The AlAs effective dielectric constant is assumed not to depend on p, as the barrier material does not undergo significant effects of confinement. Since the anisotropy of the dielectric constant components is very small when LFE's are neglected (see Figs. 8 and 9), we can consider for simplicity only one function $y_{\perp}(p)\simeq y_{\parallel}(p)\simeq y(p)$. This function can be deduced by fitting the calculated component $\varepsilon^{\mathrm{NLF}}_{\perp}$ (or $\varepsilon^{\mathrm{NLF}}_{\parallel}$). Moreover, we observe that GaAs and AlAs bulk dielectric constants both decrease by about 10% when the LFE's are included in the calculations. We make the hypothesis that the same reduction due to LFE's is found for the effective GaAs dielectric constant at any period p: $\varepsilon^{\mathrm{LF}}_{\mathrm{GaAs}}(p)=\varepsilon^{\mathrm{LF}}_{\mathrm{GaAs}}y(p)$. Within this hypothesis, we obtain the following expressions for the dielectric tensor components including LFE's, as a function of $y(p)$:

$$\varepsilon^{\mathrm{LF}}_{\perp}=\frac{1}{2}[\varepsilon^{\mathrm{LF}}_{\mathrm{GaAs}}y(p)+\varepsilon^{\mathrm{LF}}_{\mathrm{AlAs}}], \tag{17}$$

$$\varepsilon^{\mathrm{LF}}_{\parallel}=2\frac{y(p)\varepsilon^{\mathrm{LF}}_{\mathrm{GaAs}}\varepsilon^{\mathrm{LF}}_{\mathrm{AlAs}}}{y(p)\varepsilon^{\mathrm{LF}}_{\mathrm{GaAs}}+\varepsilon^{\mathrm{LF}}_{\mathrm{AlAs}}}=2\frac{\varepsilon^{\mathrm{LF}}_{\mathrm{AlAs}}}{1+[1/y(p)](\varepsilon^{\mathrm{LF}}_{\mathrm{AlAs}}/\varepsilon^{\mathrm{LF}}_{\mathrm{GaAs}})}. \tag{18}$$

By fitting $y(p)$ to *ab initio* and semiempirical dielectric constant curves, respectively, we are able to evaluate Eqs. (17) and (18) for the two cases. The results are shown as dashed lines in Figs. 8 and 9. The agreement with the calculated curves is very good in both the *ab initio* and semiempirical approaches for the in-plane component. $\varepsilon^{\mathrm{LF}}_{\perp}$ is in fact the average of the GaAs and AlAs effective dielectric constants in Eq. (17), and simply shows the confinement effects contained in the variation of $\varepsilon_{\mathrm{GaAs}}(p)$. The curves calculated including and neglecting LFE's are almost parallel, as the effect of the inclusion of LFE's is reasonably representable by a scaling factor on both bulk components at any period p.

Concerning the in-growth component, only for the semiempirical results is the agreement comparable; instead, there is an evident discrepancy between the model and the *ab initio* calculations for thin-layer SL's. Nevertheless, from Eq. (18) one can at least partially understand why the in-growth component should show less deviation from the effective medium result than the in-plane one. In fact, the ratio $\varepsilon^{\mathrm{LF}}_{\mathrm{AlAs}}/\varepsilon^{\mathrm{LF}}_{\mathrm{GaAs}}$ is smaller than unity, even when multiplied by $1/y$, so that the dominant contribution to the component is a constant with respect to the SL period.[52] Basically, the LFE for $\varepsilon^{\mathrm{LFE}}_{\parallel}$ tends to localize the field in the material with a smaller dielectric constant (AlAs in our case), which is less sensitive to confinement effects. This should be even more

true in systems with stronger dielectric mismatch, such as $GaAs/AlO_x$ or $GaAs/Al_2O_3$.

In Fig. 9 the anisotropy of the semiempirical dielectric tensor does not evolve significantly as a function of p: the two semiempirical curves $\varepsilon_{\parallel}^{\mathrm{LFE}}$ and $\varepsilon_{\perp}^{\mathrm{LFE}}$ are almost parallel. As a direct consequence, the semiempirical birefringence (see Ref. 25) remains close to the large-period limit value even in the case of thin layers, in disagreement with the experimental measurements and with the *ab initio* calculations. We observe that the only remarkable difference that we have detected between DFT-LDA and semiempirical band structures is in the electronic density along the SL growth axis (see Fig. 5): the DFT-LDA density profile shows a delocalization of the states at the interface much stronger than the one in semiempirical calculations.

The comparison of numerical results, model calculations, and measurements leads to two conclusions. First, for small periods, the DFT-LDA calculations agree with the experimental findings, but deviate from the simple model as the assumption of sharp interfaces and carriers confined in the GaAs layer is not correct. We will see later that by including in the model an interface region we can correct the in-growth component of ε and explain the discrepancy present in Fig. 8. Second, the semiempirical calculations are well reproduced by the model, but do not account for the steep rise of the birefringence in the small-p region. This reveals a limitation of the semiempirical pseudopotential approach, which does not give enough flexibility to electronic states at the interfaces. As a result, when the weight of interface states is important, the semiempirical method is not reliable, at least as for as small quantities like the birefringence are concerned. A correct description of the interface states turns out to be extremely important, as it significantly affects the anisotropy of the dielectric properties. Nevertheless, the LCBB method proves to work very well at large SL periods, when the relative weight of interfaces is less important.

In addition to the presence of an "electronic" interface region in the ideal sample, defined as the region where the wave functions do not have a precise GaAs-like or AlAs-like character, we have to consider the existence of an experimental interface region, due to the interlayer diffusion in the measured sample. This interface roughness can have an important impact on the experimental results, as we will show in the following. In fact, we evaluated approximately the effect of the atomic interlayer diffusion (unavoidable in the measured sample) at the interfaces on the LFE's, by means of a classical three-layer model. The first layer is a homogeneous dielectric with the dielectric constant of bulk GaAs, the second layer is the interface region, characterized by an unknown dielectric constant ε_I and a width equal to l_I layers, and the third layer is a homogeneous dielectric with the dielectric constant of bulk AlAs. By applying the effective medium theory,[13–15] we can extract the dielectric tensor components for such a three-layer SL:

$$\varepsilon_{\perp} = \langle \varepsilon \rangle + \frac{l_I}{p}(\varepsilon_I - \langle \varepsilon \rangle), \tag{19}$$

$$\varepsilon_{\parallel} = \frac{1}{\langle \varepsilon^{-1} \rangle}\left(1 + \frac{\rho_I \beta}{\rho \langle \varepsilon^{-1} \rangle}\right)^{-1}, \tag{20}$$

where

$$\beta = \frac{1}{\varepsilon_I} - \langle \varepsilon^{-1} \rangle \tag{21}$$

and $\langle \varepsilon^{-1} \rangle$ and $\langle \varepsilon \rangle$ are given by Eqs. (1) and (2). The fit has two parameters (l_I and ε_I), whose values can be fixed by relying on some simple physical observations. First, as it is known that the experimental sample shows at least one monolayer interdiffusion,[12] we set the experimental interface region width to two monolayers ($\lambda_I = 2$). Second, as we expect to find at the interface a GaAlAs alloy due to the interdiffusion, we assign to this region a dielectric constant ε_I equal to the average bulk dielectric constant (of course, the model starts to be valid for $p \geqslant 3$, otherwise the definition of the interface layer is meaningless). Hence, from Eq. (1) $\varepsilon_I = \langle \varepsilon \rangle$, and Eq. (19) becomes $\varepsilon_{\perp} = \langle \varepsilon \rangle$: in the direction perpendicular to the interfaces the effective medium theory always predicts a dielectric constant describing an average homogeneous medium, independent of p [unless the constituent itself changes, as simulated above by the function $y(p)$]. In the direction parallel to the interfaces, the interface region introduced in Eq. (20) has the effect of reducing the LFE's. The effect is stronger for small p and vanishes when p gets large: as a consequence, $\varepsilon_{\parallel}$ approaches the effective medium limit more slowly.

We conclude that, for thin layers, the interlayer diffusion can drastically reduce the birefringence (for $p = 3$ the effective reduction is about 60%). A larger interface region would produce a further reduction of the birefringence. This effect clearly decreases when the SL period increases and can explain, at least qualitatively, the difference still present between the DFT-LRC and the experimental birefringence (see Fig. 2 in Ref 25) in the small-period region.

Finally, it should also be noted that the reduction of LFE's due to the presence of an interface region can also be used to correct the dashed curves in Fig. 8(b): these curves were obtained by assuming sharp interfaces, whereas the existence of an interface region in the *ab initio* calculation results is clearly shown in Fig. 5. By estimating this "electronic interface" region as large as one monolayer, we can recalculate the in-growth component of ε which includes LFE's, by applying Eq. (20), provided that $\langle \varepsilon^{-1} \rangle$ in Eq. (19) is substituted by $1/\varepsilon_{\parallel}^{\mathrm{LF}}$ from Eq. (18). The result is the dotted curve in Fig. 8(b): the agreement with the $\varepsilon_{\parallel}$ calculated in the RPA is strongly improved, leading to a model $\varepsilon_{\parallel}$ close to its effective medium value.

VII. CONCLUSIONS

We calculated the dielectric tensor components and the optical absorption spectra of (001) $(GaAs)_p/(AlAs)_p$ SL's as a function of the period within time-dependent density functional theory. The band structures were obtained by means of density functional theory in the local density approximation and by the semi-empirical linear combination of bulk bands method. The analysis of the macroscopic dielectric tensor as a function of the barrier and well width, from the monolayer ($p = 1$) SL up to large supercell sizes ($p = 14$) and the comparison to available experimental data show that only *ab initio* calculations are reliable in the case of thin layers. In

both approaches, for large-scale systems, the dielectric constant components converge to the classical limits predicted by the effective medium theory. The anisotropy of the dielectric properties is explained as governed by the interplay between quantum confinement and crystal local field effects. A quantitative calculation of the birefringence is very difficult as this quantity is very small and extremely sensitive to the interface properties. In particular, for small-scale heterostructures, when the relative weight of interface states is more important, the semiempirical method does not provide a satisfying description of the anisotropy. Further many-body effects give only quantitative corrections to the static birefringence, whereas their inclusion is crucial to obtain precise spectra. In particular, we examined the effects of a static long-range contribution, due to the electron-hole interaction, to the exchange correlation kernel of DFT, showing that this approximation works very well for semiconducting SL's, and thus providing a first step for the extension of the limits of validity of this approach to more complex systems.

ACKNOWLEDGMENTS

The authors thank Miguel Marques for his useful suggestions and comments. Ground state calculations were performed using the PWSCF program.[53] TDDFT calculations were done by using the DP code.[54] Computer time was granted by IDRIS (Project No. 020544) on the NEC SX5. Part of this work has been supported by the European Commission Contract No. NANOPHASE HPRN-CT-2000-00167. S.B. was supported by the Marie Curie Actions of the European Commission, Contract No. IHP-MPMF-CT-2002-01793.

*Electronic address: silvana.botti@polytechnique.fr

[1] M. Garriga, M. Cardona, N. E. Christensen, P. Lautenschlager, T. Isu, and K. Ploog, Phys. Rev. B **36**, 3254 (1987).
[2] O. Günther, C. Janowitz, G. Jungk, B. Jenichen, R. Hey, L. Däweritz, and K. Ploog, Phys. Rev. B **52**, 2599 (1995).
[3] U. Schmid, N. E. Christensen, M. Cardona, F. Luke, and K. Ploog, Phys. Rev. B **45**, 3546 (1992).
[4] K. B. Kahen and J. P. Leburton, Phys. Rev. B **33**, 5465 (1986).
[5] J. B. Xia and Y. C. Chang, Phys. Rev. B **42**, 1781 (1990).
[6] R. G. Dandrea and A. Zunger, Phys. Rev. B **43**, 8962 (1991).
[7] E. Ghahramani, D. J. Moss, and J. E. Sipe, Phys. Rev. B **43**, 9269 (1991).
[8] Y. E. Kitaev, A. G. Panfilov, P. Tronc, and R. A. Evarestov, J. Phys.: Condens. Matter **9**, 257 (1997).
[9] E. H. Li, J. Appl. Phys. **82**, 6251 (1997).
[10] S. S. Li and B. F. Zhu, J. Phys.: Condens. Matter **10**, 6311 (1998).
[11] A. Fiore, V. Berger, E. Rosencher, P. Bravetti, and J. Nagle, Nature (London) **391**, 463 (1998).
[12] A. A. Sirenko, P. Etchegoin, A. Fainstein, K. Eberl, and M. Cardona, Phys. Rev. B **60**, 8253 (1999).
[13] D. J. Bergman, Phys. Rep. **43**, 377 (1978).
[14] M. G. Cottam and D. R. Tilley, in *Introduction to Surface and Superlattice Excitations*, Proceedings of the International School of Physics "Enrico Fermi," Course XXXIV, edited by J. Tauc (Cambridge University Press, Cambridge, England, 1989), p. 267.
[15] E. Jahne, Phys. Status Solidi B **194**, 279 (1996).
[16] P. Hohenberg and W. Kohn, Phys. Rev. **136**, B864 (1964).
[17] W. Kohn and L. J. Sham, Phys. Rev. **140**, A1133 (1965).
[18] See, e.g., D. M. Wood and A. Zunger, Phys. Rev. B **53**, 7949 (1996); A. Franceschetti and A. Zunger, *ibid.* **52**, 14664 (1995).
[19] L. W. Wang, A. Franceschetti, and A. Zunger, Phys. Rev. Lett. **78**, 2819 (1997).
[20] S. B. Zhang, M. S. Hybertsen, M. L. Cohen, S. G. Louie, and D. Tomanek, Phys. Rev. Lett. **63**, 1495 (1989).
[21] M. Alouani, S. Gopalan, M. Garriga, and N. E. Christensen, Phys. Rev. Lett. **61**, 1643 (1988).
[22] S. Botti and L. C. Andreani, Phys. Rev. B **63**, 235313 (2001).
[23] M. Rohlfing and S. G. Louie, Phys. Rev. Lett. **81**, 2312 (1998).
[24] S. Botti, F. Sottile, N. Vast, V. Olevano, H.-C. Weissker, L. Reining, A. Rubio, G. Onida, R. DelSole, and R. W. Godby, Phys. Rev. B **69**, 155112 (2004).
[25] S. Botti, N. Vast, L. Reining, V. Olevano, and L. C. Andreani, Phys. Rev. Lett. **89**, 216803 (2002).
[26] E. K. U. Gross and W. Kohn, Phys. Rev. Lett. **55**, 2850 (1985).
[27] E. K. U. Gross and W. Kohn, Phys. Rev. Lett. **57**, 923 (1986).
[28] L. Reining, V. Olevano, A. Rubio, and G. Onida, Phys. Rev. Lett. **88**, 066404 (2002).
[29] See, e.g., D. M. Bylander and L. Kleinman, Phys. Rev. B **34**, 5280 (1986); D. M. Wood, S.-H. Wei, and A. Zunger, *ibid.* **37**, 1342 (1988); B. I. Min, S. Massidda, and A. J. Freeman, *ibid.* **38**, 1970 (1988); S. Baroni, P. Giannozzi, and E. Molinari, *ibid.* **41**, 3870 (1990).
[30] D. R. Hamann, Phys. Rev. B **40**, 2980 (1989).
[31] N. Troullier and J. L. Martins, Phys. Rev. B **43**, 1993 (1991).
[32] J. P. Perdew and A. Zunger, Phys. Rev. B **23**, 5048 (1981).
[33] D. M. Ceperley and B. J. Alder, Phys. Rev. Lett. **45**, 566 (1980).
[34] M. Fuchs, M. Bockstedte, E. Pehlke, and M. Scheffler, Phys. Rev. B **57**, 2134 (1998), and references therein.
[35] S. Baroni and R. Resta, Phys. Rev. B **33**, 7017 (1986), and references therein.
[36] S. G. Louie, S. Froyen, and M. L. Cohen, Phys. Rev. B **26**, 1738 (1982).
[37] *Numerical Data and Functional Relationships in Science and Technology*, edited by K. H. Hellwege, Landolt-Börnstein, New Series, Group III, Vol. 17 (Springer-Verlag, Berlin, 1982).
[38] K. A. Mäder and A. Zunger, Phys. Rev. B **50**, 17393 (1994).
[39] R. W. Godby, M. Schlüter, and L. J. Sham, Phys. Rev. B **35**, 4170 (1987).
[40] It must be remarked that here the definition of "heavy hole" and "light hole" bands is not the most usual one. In fact, if spin-orbit interaction is included, the two upper valence bands are no longer degenerate except at Γ and they are designated as "heavy hole" and "light hole," while the lower single band is called "split off."
[41] W. Ge, W. D. Schmidt, M. D. Sturge, L. N. Pfeiffer, and K. W. West, J. Lumin. **59**, 163 (1994).

[42] G. Li, D. Jiang, H. Han, Z. Wang, and K. Ploog, Phys. Rev. B **40**, 10430 (1989).
[43] S. B. Zhang, M. L. Cohen, and S. G. Louie, Phys. Rev. B **43**, 9951 (1991), and references therein.
[44] J. H. Burnett, Z. H. Levine, and E. L. Shirley, Phys. Rev. B **64**, 241102(R) (2001).
[45] S. L. Adler, Phys. Rev. **126**, 413 (1962).
[46] N. Wiser, Phys. Rev. **129**, 62 (1963).
[47] R. DelSole, G. Adragna, V. Olevano, and L. Reining, Phys. Rev. B **67**, 045207 (2003).
[48] R. M. Martin, J. A. V. Vechten, J. E. Rowe, and D. E. Aspnes, Phys. Rev. B **6**, 2500 (1972).
[49] We want to point out that when we applied this LRC (or equivalently contact exciton) model to study the effect of quasiparticle corrections and excitonic effects on the static birefringence Ref. 25, we did not use these value for $\alpha_{\parallel}$ and $\alpha_{\perp}$. In fact, as explained in Ref. 24, a constant α can work only for a finite range of frequencies. The values of α that correct the static dielectric constants are systematically smaller than the values of α that reproduce the absorption peaks (for the GaAs/AlAs SL about 10 times smaller). Moreover, when we are interested in the birefringence, the slight difference between in-plane $\alpha_{\perp}$ and in-growth $\alpha_{\parallel}$ can be relevant and affect the anisotropy of the dielectric response. Therefore, in that case we used two independent parameters, fitted to reproduce the experimental dielectric mismatch.
[50] L. Pavesi and M. Guzzi, J. Appl. Phys. **75**, 4779 (1994).
[51] M. S. Hybertsen and S. G. Louie, Phys. Rev. B **35**, 5585 (1987).
[52] As we will discuss later, this is not sufficient to explain why the in-growth component remains close to its effective medium value; in fact the contributions due to the delocalization of the wave functions at the interface must also be considered.
[53] S. Baroni, A. Dal Corso, S. De Gironcoli, and P. Giannozzi, http://www. pwscf. org
[54] http://theory.lsi.polytechnique.fr/codes/